Wear 268 (2010) 643–652

Contents lists available at ScienceDirect

Wear

journal homepage: www.elsevier.com/locate/wear

Analysis of planar multibody systems with revolute joint wear

Saad Mukras, Nam H. Kim*, Nathan A. Mauntler, Tony L. Schmitz, W. Gregory Sawyer

Department of Mechanical and Aerospace Engineering, University of Florida, Gainesville, FL, USA

ARTICLE INFO

Article history:
Received 31 March 2009
Received in revised form 25 August 2009
Accepted 28 October 2009
Available online 10 November 2009

Keywords:
Wear prediction
Finite element method
Joint clearance
Slider-crank
Multibody dynamics

ABSTRACT

Wear prediction on the components of a mechanical system without considering the system as a whole will, in most cases, lead to inaccurate predictions. This is because the wear is directly affected by the system dynamics which evolves simultaneously with the wear. In addition, the contact condition (regions of contact for the wearing bodies) also depends on the system dynamics and can only be determined in a multibody dynamics framework.

In this work, a procedure to analyze planar multibody systems in which wear is present at one or more revolute joints is presented. The analysis involves modeling multibody systems with revolute joints that consist of clearance. Wear can then be incorporated into the system dynamic analysis by allowing the size and shape of the clearance to evolve as dictated by wear. An iterative wear prediction procedure based on Archard's wear model is used to compute the wear as a function of the evolving dynamics and tribological data. The procedure is then validated by comparing the wear prediction with wear on an experimental slider-crank mechanism.

1. Introduction

The presence of clearances in the joints of mechanical systems has been noted to retard system performance. Often, vibration, noise, and joint reaction forces characterized by large instantaneous values are experienced as a consequence of joint clearance. The problem is further compounded when the clearance size is increased and its shape altered by wear. This has generated interest over the past three decades to develop ways to account for the effect of joint clearance. Early studies in this area focused on simple models to obtain insight into the behavior of systems with joint clearances. Dubowsky et al. [1,2] developed a contact impact pair model to study the elastic joint with clearance. In their model, joint elasticity and damping were modeled via springs and a viscous coefficient. Dubowsky and Gardner [3] later extended this work to include flexible mechanism as well as multiple clearance connections. Earles and Wu [4] proposed to model joint clearance using a massless rigid link whose length was equal to the clearance size. The components of the joint were thus assumed to be in contact at all times. Wu and Earles [5] later used the model to predict contact loss between the joint components for a planar mechanism. The concept of a massless link was also used by Furuhashi et al. [6–9] to study the dynamics of a four-bar linkage with clearance. Once again, the joint components were assumed to be in contact at all times.

More complex models have also been developed to study the effect of clearance on system dynamics. Considering the joint to consist of two components, Farahanchi and Shaw [10] modeled joint clearance by considering three configurations of the joint components: (1) free-flight motion, when the components are not in contact; (2) the impact condition, when the components establish contact; and (3) the sliding condition, when the components are in contact and in relative motion. In their model, the reaction force at the joint (when the joint components are in contact) was determined by assuming that no clearance was present. They used a slider-crank mechanism to demonstrate the procedure and studied the effect of clearance size, friction, crank speed and impact parameters. Rhee and Akay [11] also used the three modes of motion to model the joint clearance. They used an approach similar to that of Farahanchi and Shaw [10] to determine the reaction force during the sliding motion. They studied the response of a four-bar mechanism with clearance in a revolute joint.

The three-mode approach was also used by Khulief and Shabana [12] to model the clearance at a joint. In their approach, termed as the discontinuous method, the analysis (integration of the equations of motion) is divided into two parts, namely, pre- and post-collision, where a momentum balance is performed to determine the post-collision velocities. Velocities in the analysis are then updated and the analysis is resumed.

Ravn [13] also implemented the three-mode approach to model the joint clearance. However, in his approach, the reaction force

* Corresponding author at: Department of Mechanical & Aerospace Engineering, University of Florida, 210 MAEA, PO Box 116250, Gainesville, FL 32611-6250, USA. Tel.: +1 352 846 0665; fax: +1 352 392 7303.
E-mail addresses: mukras@ufl.edu (S. Mukras), nkim@ufl.edu (N.H. Kim), mauntler@ufl.edu (N.A. Mauntler), tschmitz@ufl.edu (T.L. Schmitz), wgsawyer@ufl.edu (W.G. Sawyer).

0043-1648/$ – see front matter © 2009 Elsevier B.V. All rights reserved.
doi:10.1016/j.wear.2009.10.014

Nomenclature

A	contact area
A_E	extrapolation factor
δ	penetration
e_r	coefficient of restitution
E	Young's modulus
$\mathbf{F}_N$	normal force in the contact interface
h	wear depth
$\boldsymbol{k}$	dimensioned wear coefficient
K	elastic constant
$\boldsymbol{\lambda}$	vector of Lagrange multipliers
$\mathbf{M}$	mass matrix
p	contact pressure
$\mathbf{q}$	vector of generalized coordinates
$\mathbf{Q}^A$	vector of applied loads
s	sliding distance
t	time
υ	Poisson's ratio
$\boldsymbol{\Phi}$	constraint vector
$\boldsymbol{\Phi}_\mathbf{q}$	Jacobian matrix
ω	Crank velocity

during the impact and sliding mode is computed using a contact force model. This analysis has been termed the continuous method since integration of the equations of motion is not halted as in the case of the discontinuous method. A number of researchers [14–18] have since used this technique to model and study the effect of clearance in the joints of multibody systems.

This prior research has focused on modeling multibody systems with joint clearance that remains constant. However, in some mechanical systems, especially close-loop dynamic systems, wear in the joints significantly affects system dynamics, and the change in system dynamics greatly affects the wear progress. In such a case, it is essential to predict the joint wear in the multibody framework. The work described here seeks to complement these previous studies by integrating wear into the dynamic analysis of multibody systems. In doing so, the effect of the evolving system kinematics (due to wear) can be modeled. The first part of the paper presents a discussion on the dynamic analysis of a planar multibody system with joint clearance (i.e., a non-ideal joint). A prediction procedure to estimate wear on simple geometries, such as a revolute joint, is then presented. Next, analysis of multibody systems with revolute joint wear, which involves integrating wear prediction into the dynamic analysis, is discussed. The analysis procedure is then validated by modeling a slider-crank mechanism with single joint wearing and comparing the predictions with wear on an experimentally equivalent mechanism. Finally, an example that demonstrates the necessity for using a multibody dynamics framework for wear prediction is presented.

2. Analysis of multibody systems with non-ideal joints

The analysis of a multibody systems requires the assembly and solution of a set of Differential Algebraic Equations (DAE) of motion that describe the motion of the system. This is true for systems with ideal joints (no clearance) as well as systems with non-ideal joints (including clearance). The only difference in analyzing systems with non-ideal joints, as opposed to those with ideal joints, is in the description of the joint. Thus, in this section, a brief discussion of the equations of motion will be presented followed by a discussion on modeling a non-ideal joint.

2.1. Equations of motion for multibody systems

A multibody system is defined as consisting of a set of interconnected rigid bodies that undergo large displacements and rotations. Tracking the motion of body i in a global coordinate system (x–y) is achieved by fixing a reference frame (x_i'–y_i') on each body. Body i in the system can then be located by specifying the origin of the corresponding body-fixed coordinates expressed as

$$\mathbf{q}_i = [x, y, \phi]_i^T. \tag{1}$$

In Eq. (1), ϕ denotes the relative angle between the body's reference frame and the global coordinate system (i.e., orientation). Thus, for a multibody system a set of generalized coordinates, as shown in Eq. (2), uniquely define the position and orientation of all bodies in the system.

$$\mathbf{q} = [[x, y, \phi]_1^T, [x, y, \phi]_2^T, \ldots, [x, y, \phi]_i^T]^T. \tag{2}$$

The bodies in a multibody system are interconnected by joints which impose conditions on their relative motion. Consequently, the generalized coordinates are usually not independent. When these conditions are expressed as algebraic equations in terms of the generalized coordinates and time, t, they are referred to as holonomic kinematic constraints [20] and are expressed as

$$\boldsymbol{\Phi}(\mathbf{q}, t) = \mathbf{0}. \tag{3}$$

Assuming that the multibody system of interest is properly constrained and the number of constraints equal the generalized coordinates, Eq. (3) can simultaneously be solved to uniquely determine the position, $\mathbf{q}$, of the system components at any time. Furthermore, the velocities and acceleration of all components can be determined using Eqs. (4) and (5):

$$\boldsymbol{\Phi}_\mathbf{q}\dot{\mathbf{q}} = -\boldsymbol{\Phi}_t, \tag{4}$$

$$\boldsymbol{\Phi}_\mathbf{q}\ddot{\mathbf{q}} = -(\boldsymbol{\Phi}_\mathbf{q}\dot{\mathbf{q}})_\mathbf{q}\dot{\mathbf{q}} - 2\boldsymbol{\Phi}_{\mathbf{q}t}\dot{\mathbf{q}} - \boldsymbol{\Phi}_{tt} \equiv \boldsymbol{\gamma}. \tag{5}$$

These equations are obtained by differentiating Eq. (3) with respect to time.

The solution of the constraint, velocity, and acceleration equations to determine the motion of the system is referred to as kinematic analysis. In order to determine the system response due to externally applied loads, it is necessary to perform a dynamic analysis. As discussed previously, this requires the assembly and solution of the differential algebraic equations of motion. The equations of motion for a constrained rigid multibody system are stated here without derivation due to the length and complexity of their derivations. The interested reader is referred to the work of Haug [20] for a detailed derivation of these equations using the Lagrangian approach. The equation can be expressed as

$$\mathbf{M}\ddot{\mathbf{q}} + \boldsymbol{\Phi}_\mathbf{q}^T\boldsymbol{\lambda} = \mathbf{Q}^A \tag{6}$$

where $\mathbf{M}$ is the mass matrix consisting of masses and moments of inertia for the system components, $\ddot{\mathbf{q}}$ and $\boldsymbol{\Phi}_\mathbf{q}^T$ are the acceleration vector and Jacobian of the constraints, respectively, $\boldsymbol{\lambda}$ is a vector of Lagrange multipliers, and $\mathbf{Q}^A$ is a vector of externally applied loads. In this work the body-fixed coordinate system is selected to be at the center of mass (COM) of the corresponding body. This significantly simplifies the general form of the equations of motion. The product of the Jacobian and the vector of Lagrange multipliers ($\boldsymbol{\Phi}_\mathbf{q}^T\boldsymbol{\lambda}$) is in fact the vector of reaction forces. This is the second term on the left hand side of Eq. (6). For an unconstrained system, the vector of Lagrange multipliers is zero and this term disappears.

Eqs. (5) and (6) can be combined to result in a mixed system of Differential Algebraic Equations (DAE) of motion. The equations

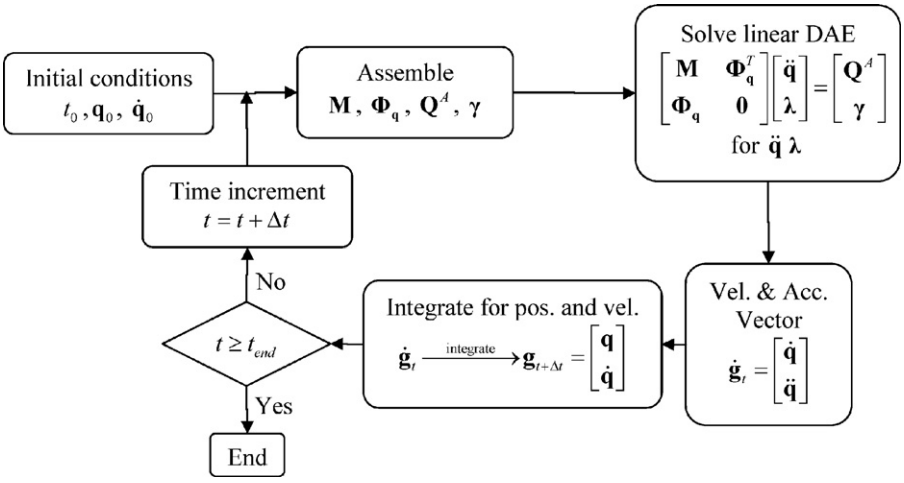

Fig. 1. Integration procedure for the Differential Algebraic Equation.

are expressed as

$$\begin{bmatrix} \mathbf{M} & \boldsymbol{\Phi}_\mathbf{q}^T \\ \boldsymbol{\Phi}_\mathbf{q} & \mathbf{0} \end{bmatrix} \begin{bmatrix} \ddot{\mathbf{q}} \\ \boldsymbol{\lambda} \end{bmatrix} = \begin{bmatrix} \mathbf{Q}^A \\ \boldsymbol{\gamma} \end{bmatrix}, \tag{7}$$

where $\boldsymbol{\gamma} = \boldsymbol{\Phi}_\mathbf{q}\ddot{\mathbf{q}} = -(\boldsymbol{\Phi}_\mathbf{q}\dot{\mathbf{q}})_\mathbf{q}\dot{\mathbf{q}} - 2\boldsymbol{\Phi}_{\mathbf{q}t}\dot{\mathbf{q}} - \boldsymbol{\Phi}_{tt}$. For a meaningful system, the coefficient matrix of Eq. (7) must be nonsingular. This is guaranteed if the mass matrix $\mathbf{M}$ is positive definite and the Jacobian matrix $\boldsymbol{\Phi}_\mathbf{q}$ is full row rank (or constraints equations are independent). The solution procedure for this equation, which determines the dynamics of a system, is well documented in the literature [14,19,20] and is only summarized in the form of a flow chart in Fig. 1.

2.2. Modeling a non-ideal revolute joint

In the previous section, the dynamic analysis of a multibody system was presented. The procedure may be applied for systems with either ideal or non-ideal revolute joints as long as the constraints are correctly formulated. The procedure for modeling a non-ideal revolute joint is presented next. It closely follows the work of Ravn [13] and Flores [17].

It is assumed that a revolute joint consists of two components, a pin and a bushing, that are rigidly attached to bodies i and j as shown in Fig. 2. Furthermore, the joint components are assumed to be compliant even though the bulk of the bodies i and j are assumed to be rigid. For an ideal revolute joint, the centers of the pin and the bushing coincide and therefore allow only a relative rotation between the two bodies. With the aid of Fig. 3 the kinematic constraint for the ideal joint can be expressed as

$$\boldsymbol{\Phi}^{r(i,j)} = (\mathbf{r}_i + \mathbf{A}_i\mathbf{s}_i) - (\mathbf{r}_j + \mathbf{A}_j\mathbf{s}_j) = \mathbf{0}, \tag{8}$$

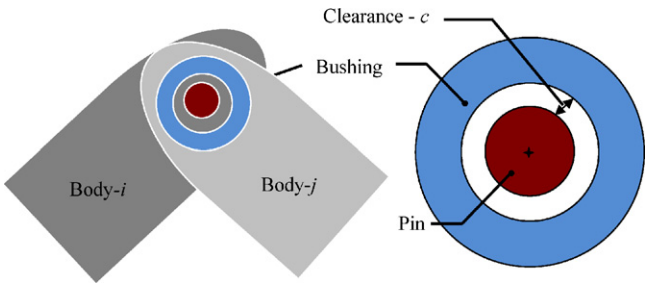

Fig. 2. A revolute joint with clearance.

where $\mathbf{r}_i$ and $\mathbf{r}_j$ are the position vectors in the global coordinate system (x–y) that describe the location of the body-fixed coordinates (x_i–y_i and x_j–y_j), the vectors $\mathbf{s}_i$ and $\mathbf{s}_j$ are position vectors in the body-fixed coordinate systems that locate the center of the revolute joint, and $\mathbf{A}_i$ and $\mathbf{A}_j$ are the matrices that transform vectors in the body-fixed coordinates systems into vectors in the global system.

In the case of a non-ideal revolute joint, a clearance is present in the joint so that the centers of the joint components (pin and bushing) no longer coincide. Instead, the pin and the bushing may have three different configurations during motion. The three configurations are: freefall, when the components are not in contact; impact; and following motion, which together describe the duration when the joint components establish and maintain contact. The non-ideal joint model can be realized by ensuring that the motion of the pin is confined within the inner perimeter of the bushing. This is achieved by imposing a force constraint on both components whenever they establish contact as discussed by Flores and Ambrósio [16]. It is assumed that the region where the contact is established is deformable so that the reaction force can be estimated by a contact force law. A contact force model with hysteresis damping, discussed by Hamid and Parviz [21], can be employed. The model is expressed as

$$F_N = K\delta^{1.5}\left(1 + \frac{3(1-e_r^2)}{4}\frac{\dot{\delta}}{\dot{\delta}^{(-)}}\right), \tag{9}$$

where F_N is the reaction force, δ is the penetration between the pin and bushing, e_r is the coefficient of restitution, δ is the penetration

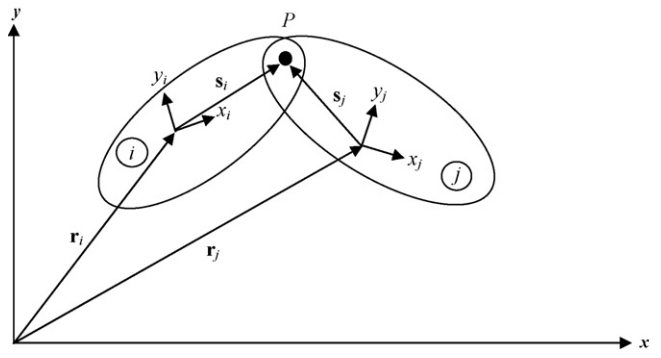

Fig. 3. Revolute joint between bodies i and j. The joint imposes a constraint on the relative translation between the bodies.

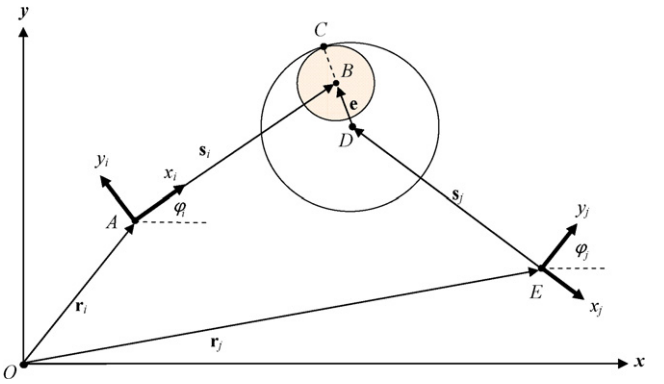

Fig. 4. Geometric description of a non-ideal revolute joint with eccentric vector **e**.

velocity, $\dot{\delta}^{(-)}$ is the initial penetration velocity upon impact and K is a constant that is dependent on the material properties of the components and their geometry. The constant is expressed as

$$K = \frac{4}{3(h_i + h_j)}\left(\frac{R_i R_j}{R_i + R_j}\right)^{1/2}, \quad h_n = \frac{1-\upsilon_n^2}{E_n}, \quad n = 1, 2, \tag{10}$$

where R_i and R_j are the radii of the pin and bushing, respectively, υ_n is Poisson's ratio of the components and E_n is the elastic modulus of the components. The radii of the pin and bushing are calculated based on wear depths at the particular contact location. In addition to the reaction forces, a friction force can be included to enhance the model. In this work, Coulomb friction is applied. The friction force is

$$F_f = \mu F_N, \tag{11}$$

where μ is the coefficient of friction which can be determined through experiments as discussed by Schmitz et al. [22] and F_N is the normal force.

The contact model shown in Eq. (9) is valid for colliding spheres whose contact area is circular. While several expressions have been proposed to model the colliding cylinders [2,43], this model has been used in multibody dynamic analysis by a number of researchers [13,16] to estimate the contact force between colliding cylinders. The justification for using the expression in Eq. (9) is that the proposed models for cylindrical contact are nonlinear implicit expressions of the contact force F_N whose results do not differ substantially from the expression in Eq. (9) when R_i and R_j are replaced with the cylinder radii. A more detailed discussion of the justification is presented in the literature [13,16,17]. In this work the model in Eq. (9) is used to estimate the contact force at the revolute joint. It will be shown that the model yield similar results to experiments when used in multibody analysis.

In order to apply the constraint force, it is necessary to determine the location of contact between the joint components, the direction in which the contact force is acting and the penetration. To determine this information, Fig. 4 is employed. The figure shows two bodies constrained by a non-ideal revolute joint. Body coordinates x_i–y_i and x_j–y_j are fixed to the center of masses of the bodies i and j, respectively. The coordinates are oriented at angles ϕ_i and ϕ_j relative to the global x-axis. The point of contact C is defined as the center of the contact region between the pin and the bushing. This point can be located using the eccentric vector **e** which is a vector connecting the bushing center D and the pin center B. At the time of contact the eccentric vector will point in the direction of the contact. This vector is expressed as

$$\mathbf{e} = (\mathbf{r}_i + \mathbf{A}_i\mathbf{s}_i) - (\mathbf{r}_j + \mathbf{A}_j\mathbf{s}_j), \tag{12}$$

where $\mathbf{r}_i$ and $\mathbf{r}_j$ are the vectors linking the global origin and the center or masses of the bodies, $\mathbf{s}_i$ and $\mathbf{s}_j$ are vectors in the local coordinate system that link the center of masses to the pin and bushing centers, respectively, and $\mathbf{A}_i$ and $\mathbf{A}_j$ are matrices that transform a vector from the local coordinate system to the global system. In this case, they transform vectors $\mathbf{s}_i$ and $\mathbf{s}_j$ into their global equivalent. The location of contact point C with respect to the pin and bushing can then be expressed as

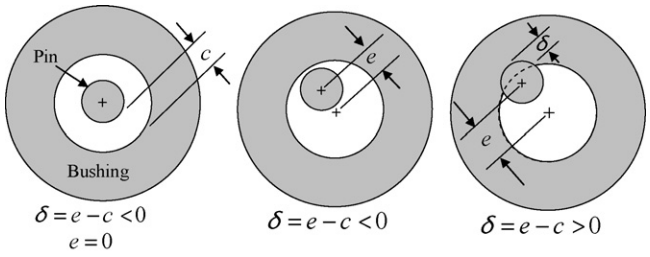

Fig. 5. Penetration during contact between the pin and the bushing.

$$\mathbf{r}_m^C = \mathbf{r}_m + \mathbf{A}_m\mathbf{s}_m + R_m\mathbf{n}, \quad m = i, j. \tag{13}$$

In Eq. (13) R_m are the radii of the pin and bushing after wear and **n** is a unit vector in the direction of **e**, which is written as

$$\mathbf{n} = \frac{\mathbf{e}}{e}. \qquad e = ||\mathbf{e}|| \tag{14}$$

The penetration between the pin and bushing during contact is computed as the difference between the eccentricity and clearance:

$$\delta = e - c. \tag{15}$$

The clearance is defined as the difference between the bushing and pin radii, $c = R_j - R_i$. When the pin is not in contact with the bushing, the eccentricity is smaller than the clearance and the penetration has a negative value. When the penetration has a value equal or greater than zero, contact is established. Thus, when δ is greater than zero, a contact force is applied between the bodies. The contact force vanishes when δ is equal to or less than zero. These configurations are depicted in Fig. 5.

To determine the contact force (see Eq. (9)), the relative penetration velocity is also required. This is the difference between the velocities of the contact point. The two velocities are

$$\dot{\mathbf{r}}_m^C = \dot{\boldsymbol{r}}_m + \boldsymbol{A}_{m,\phi_m}\dot{\phi}_m\mathbf{s}_m + R_m\dot{\boldsymbol{n}}, \quad m = i, j. \tag{16}$$

The relative velocities in the normal and tangential direction can then be computed as

$$v_n = (\dot{\boldsymbol{r}}_i^C - \dot{\boldsymbol{r}}_j^C)\cdot\boldsymbol{n} \qquad v_t = (\dot{\boldsymbol{r}}_i^C - \dot{\boldsymbol{r}}_j^C)\cdot\boldsymbol{n}^{\perp}, \tag{17}$$

where $\mathbf{n}^{\perp}$ is the unit tangent vector defined as $\boldsymbol{n}^{\perp} = \hat{\boldsymbol{k}} \times \boldsymbol{n}$ and $\hat{\boldsymbol{k}}$ is the unit vector in the global z-coordinate. In Eq. (17), the normal velocity v_n is identical to the relative penetration velocity $\dot{\delta}$; it is positive during the penetration period and negative during the rebound period.

After the relative penetration and velocity have been determined, the contact and friction forces can be computed and included in the DAE as externally applied loads. Then, the system dynamics can be determined. It is noted, however, that since the body-fixed coordinates were fixed at the center of masses of bodies i and j, the forces must also be applied at these locations rather than at the points of contact. Thus, the transfer of the loads to the mass centers will result in an addition moment in each body. The force acting at the center of mass for body i and the corresponding moment equations are expressed as

$$\boldsymbol{F}_i = -(\boldsymbol{F}_N + \boldsymbol{F}_\mu) \qquad \boldsymbol{m}_i = (\boldsymbol{F}_i)\times(\boldsymbol{r}_i^C - \boldsymbol{r}_i), \tag{18}$$

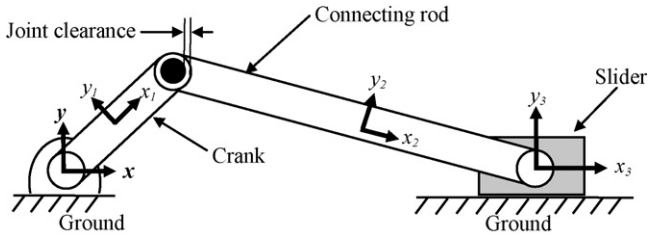

Fig. 6. Slider-crank mechanisms with joint clearance.

Table 1
Dimensions and mass parameters for slider-crank mechanism.

	Length (m)	Mass (kg)	Moment of inertia (kg m^2)
Crank	1.00	25.00	45.00
Follower	1.75	35.00	35.00
Slider	–	25.00	–

where

$$\boldsymbol{F}_N = F_N \boldsymbol{n}$$
$$\boldsymbol{F}_\mu = \mu_k F_N \boldsymbol{n}^\perp. \tag{19}$$

The corresponding loads for body j are

$$\boldsymbol{F}_j = \boldsymbol{F}_N + \boldsymbol{F}_\mu$$
$$\boldsymbol{m}_j = (\boldsymbol{F}_j) \times (\boldsymbol{r}_j^C - \boldsymbol{r}_j). \tag{20}$$

Once the forces (contact and friction forces) for the non-ideal revolute joint are known, the description of the joint is complete. It should be noted that no kinematic constraint was introduced while describing the non-ideal joint. Instead, force constraints were used in the description. As a result, a multibody system with this type of non-ideal revolute joint has two additional degrees-of-freedom that are treated using the force constraints.

2.3. Example: slider-crank mechanism with a non-ideal revolute joint

The use of the non-ideal revolute joint model will be demonstrated by modeling and performing a dynamic analysis on a slider-crank mechanism that has a non-ideal joint. Fig. 6 shows a diagram of the slider-crank mechanism which consists of four components (ground, crank, follower, and slider). The components are connected to each other by three revolute joints and a translational joint. For this example, the revolute joint between the crank and the follower is modeled as a non-ideal joint. The dimension and mass properties for the mechanism are shown in Table 1. Also, the radii and material properties for the joint components (the pin and bushing) are shown in Table 2. In this case a steel pin and a steel bushing are used. For the contact force model, a value of 0.15 and 0.8 were used for the friction coefficient and the coefficient of restitution, respectively. It is assumed in this analysis that the pin and the bushing are rigidly attached to the crank and the follower, respectively. The crank is assumed to rotate at a constant angular velocity of 30 rpm (π rad/s).

The kinematic constraint equations for this mechanism can be obtained through procedures described by Nikravesh [19] and Haug [20]. For this mechanism the constraint equations are as follows:

$$\boldsymbol{\Phi} = \begin{bmatrix} x_1 - l_1 \cos\phi_1 \\ y_1 - l_1 \sin\phi_1 \\ x_2 - x_3 + l_2 \cos\phi_2 \\ y_2 - y_3 - l_2 \sin\phi_2 \\ y_3 \\ \phi_3 \\ \phi_1 - \omega t \end{bmatrix} = \begin{bmatrix} 0 \\ 0 \\ 0 \\ 0 \\ 0 \\ 0 \\ 0 \end{bmatrix}. \tag{21}$$

In Eq. (21), the first two expressions model the revolute joint between the crank and the ground, while the third and fourth model the revolute joint between the follower and the slider. The fifth and sixth expressions model the translational motion of the slider. The final expression is the driving constraint that specifies the constant angular velocity of the crank.

It is noted that no constraint for the joint with clearance appears in Eq. (21). Instead a force constraint as previously described is used to restrict the motions of the crank relative to the follower. The Differential Algebraic Equations of motion in Eq. (7) can be assembled and solved to determine the dynamics of the system. Fig. 7 shows representative results from the dynamic analysis of the mechanism. In the figure a comparison of the joint reaction forces between the ideal and the non-ideal joints is shown for two different sizes of

Table 2
Material properties for the joint components.

	Pin	Bushing
Young's modulus	206.8 GPa	206.8 GPa
Poison's ratio	0.29	0.29
Radius	20 mm	{20.0005, 25} mm

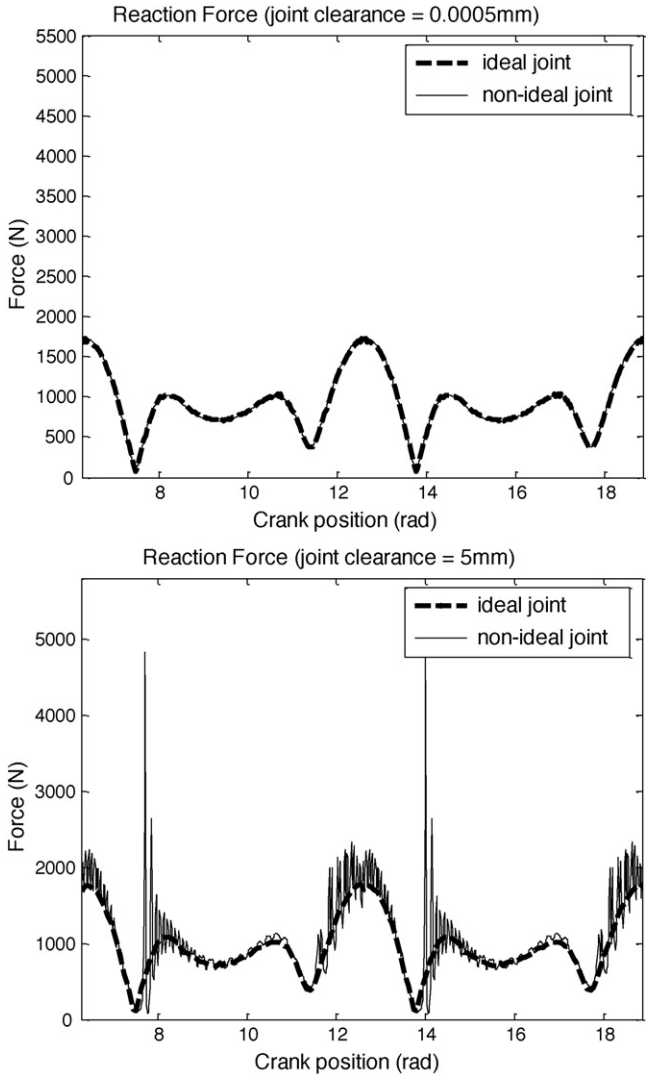

Fig. 7. Comparison of reaction forces between the ideal and the non-ideal joints for various sizes of clearance.

the joint clearance. In the first diagram the clearance size is 0.5 μm. For this case the reaction forces from the ideal and non-ideal joint models are almost identical; this is since the clearance is effectively zero. As the clearance is increased to 5 mm, the change in the system dynamics becomes evident.

3. Wear prediction

When the two components of a non-ideal joint are in contact and in relative motion, the joint is expected to wear. An enormous amount of effort has been placed into developing techniques to predict wear. A general trend that has emerged is the use of Archard's wear model [23–34] in an iterative procedure. Archard's model is a linear wear model that estimates wear based on information about the contact condition (contact pressure and sliding distance) and tribological data that reflects information about the materials in contact and the operating conditions. Thus, wear procedures typically involve an iterative process in which incremental wear is estimated at each iteration (based on the wear model) and accumulated up to the desired number of iterations.

In earlier prediction procedures, the linear extrapolation method was employed to estimate the worn geometry based on initial contact conditions. The procedures assumed that the geometry and thus contact pressure did not evolve with wear. Thus only a single iteration was required in which linear extrapolations were applied to determine the final geometry, i.e., the geometry that would result after many iterations. This procedure has been found to produce erroneous results [23,24]. The primary reason for the inaccuracy is that the evolution of the geometry was neglected.

In iterative procedures, wear predictions have been based on evolving contact conditions. The procedures allow the contact geometry to vary gradually and provide an iterative procedure in which the contact pressure and the sliding distance are computed at each iteration. The geometry is also updated at each iteration to reflect the geometry evolution. Depending on the effectiveness of the geometry update and the accuracy of the contact pressure calculations, the iterative procedures have been found to yield useful results [25–29]. The procedure has been used in wear prediction of gears [30–32], cam-followers [33–35], knee joints [36], and hip joints [37,38]. The iterative scheme has also been adopted here.

Archard's wear model has been expressed in various forms depending on the intended application. For the present work, a useful form of the model is

$$\frac{h}{s} = kp, \tag{22}$$

where h is the wear depth, s is the relative sliding distance between the two bodies in contact, k is a wear coefficient, and p is the contact pressure resulting from the contact of the concerned bodies. When two contacting bodies are composed of different materials, different wear coefficients for each body must be used in Eq. (22). The wear process may be expressed as a dynamic process (rate of change of the wear depth with respect to the sliding distance) so that the differential form of Eq. (22) can be written as

$$\frac{dh}{ds} = kp(s). \tag{23}$$

In Eq. (23), the wear depth may be estimated using a finite difference approach. Using a temporal discretization of the relative motion of the bodies in contact (the sliding distance is considered as time in the dynamic analysis) yields the updating formula:

$$h_i = h_{i-1} + kp_i\ \Delta s_i. \tag{24}$$

where Δs_i is the incremental siding distance, p_i and h_i are the contact pressure and wear depth at the ith cycle, and h_{i-1} is the wear depth at the previous cycle. Once the wear coefficient, the contact pressure, and the incremental sliding distance are available, the overall wear depth can be estimated. The wear coefficient is generally determined through experiments [25,39,40], while the contact pressure may be calculated using finite element analysis (FEA) or simplified methods such as the Winkler surface model [27]. The FEA method is used here because it can accurately (relatively) represent the complicated contact surface which may be observed during geometry evolution. The incremental sliding distance can also be obtained from FEA or may be specified explicitly. In this work it is determined from the dynamic analysis as discussed later.

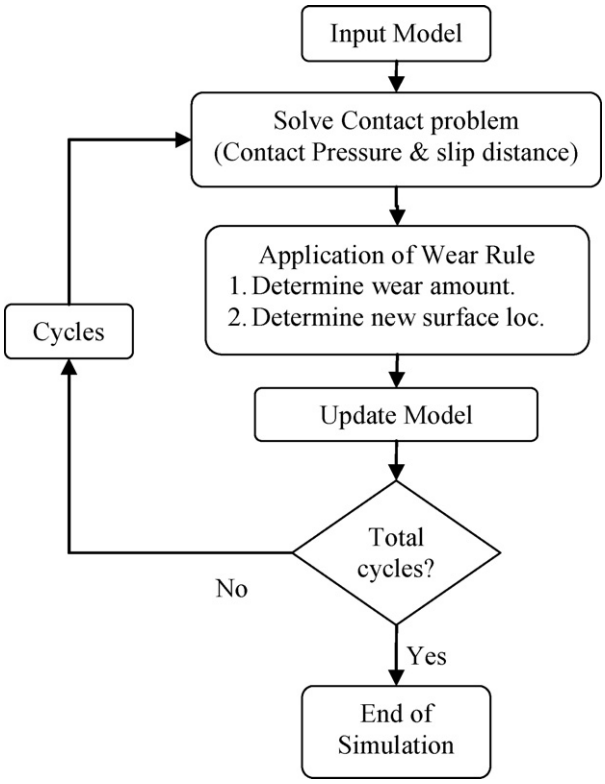

Fig. 8. Incremental wear simulation flow chart.

Proper wear predictions require that the geometry is updated to reflect the evolving contact conditions. This may be achieved by moving the contact surface in the direction of the surface normal by an amount equal to the incremental wear depth (the last term in Eq. (24)). Furthermore, since numerous cycles (the incremental wear depth during one cycle of motion is usually microscopic) may have to be simulated, it is necessary to reduce computational costs in repeated wear calculations. A popular technique in mitigating costs is the use of extrapolation. This involves calculating the incremental wear depth for a representative cycle and then extrapolating this wear depth over a preselected number of cycles. In order to incorporate extrapolation in Eq. (24), it is written as

$$h_i = h_{i-1} + kA_E p_i\, \Delta s_i, \tag{25}$$

where A_E is the extrapolation factor. In selecting a value for the extrapolation it is important to note that a large value may compromise the accuracy of the simulation since the geometry is not allowed to gradually evolve. On the other hand, using an overly conservative (small) value will result in a less than optimum use of resources. A more comprehensive study on the use of extrapolation is available in the literature [41].

The wear prediction procedure is summarized in the flowchart shown in Fig. 8. The procedure is later integrated into the dynamic analysis of mechanism with wear at the revolute joints.

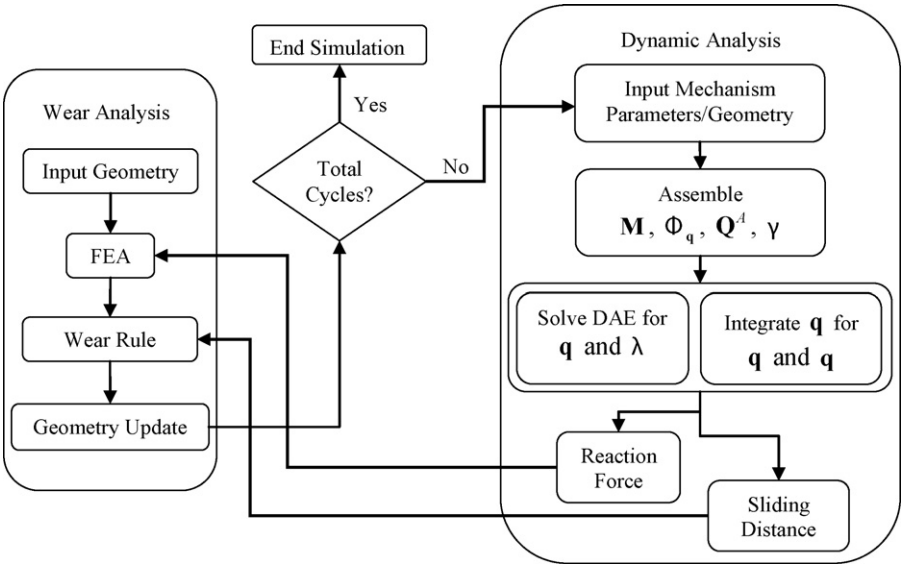

Fig. 9. Integration of wear analysis into system dynamics analysis.

4. Integration of wear model into dynamic analysis

In Section 2, a procedure to analyze multibody systems with joint clearance was presented. The procedure accounts for the changes in the system dynamics when the joint clearance is varied. It also allows for the contact location, between the joint components, to be determined at any time during the motion of the system. A wear prediction procedure to estimate the wear occurring between two bodies in contact and relative motion (such as a revolute joint) was also presented in Section 3. This procedure can be integrated into the dynamic analysis of a multibody system in order to gain insight into the overall performance of a system when wear is present at one or more of its revolute joints. The integrated model is composed of two parts: dynamic analysis and wear analysis. The model is discussed in the following subsections.

4.1. Dynamic analysis with non-ideal joints

In the first part of the integration process a dynamic analysis is performed to determine the joint reaction force (magnitude as well as direction) and the incremental sliding distance. These are the two quantities required (from the dynamic analysis) to perform a wear analysis. The analysis is performed for a complete cycle and the reaction force as well as the incremental sliding distance is obtained at each time increment of the discretized range. The reaction force at the non-ideal joint is determined by the contact force model. Thus for a non-ideal joint b the contact and friction force at time increment t_i is expressed as

$$\begin{aligned} \boldsymbol{F}^b_{N,t_i} &= F_{N,t_i}\boldsymbol{n}_{,t_i} \\ \boldsymbol{F}^b_{\mu,t_i} &= \mu_k F_{N,t_i}\boldsymbol{n}^{\perp}_{,t_i} \end{aligned}, \tag{26}$$

where F_N is the contact force and $\mathbf{n}$ is a unit normal vector pointing in the direction of contact. F_N and $\mathbf{n}$ are describe in Eqs. (9) and (14), respectively. The values of F_N and $\mathbf{n}$ are computed during the integration of the equations of motion. The incremental sliding distance is also obtained at each increment:

$$\Delta s_{t_i} = R_j \cdot (\alpha_{t_i} - \alpha_{t_{i-1}}), \tag{27}$$

where R_j is the bushing radius, α_{t_i} is the angle difference (in radians) between the local x-axis of the two bodies i and j that share a revolute joint (see Fig. 4) at a current time, and $\alpha_{t_{i-1}}$ corresponds to the difference at a previous time. The value of α_t is obtained from $\alpha_t = \phi_i - \phi_j$.

4.2. Wear analysis

Wear analysis is the second part of the integration process. The amount of wear is determined at each increment based on the reaction force and sliding distance from the previous dynamic analysis. The reaction force at each time increment is used to determine the contact pressure (through a finite element analysis) between the joint components (pin and bushing). Incremental wear can then be computed and the geometry updated.

The wear prescribed by geometry update increases the clearance. The inner perimeter of the bushing is altered from its circular shape to one dictated by the wear. This implies that the value of c in Eq. (15) is no longer a constant value and instead depends on the location of contact C (as defined in Fig. 4 and Eq. (13)). Thus, the value of c must also to be updated during the dynamic analysis:

$$c = ||\boldsymbol{r}_B - \boldsymbol{r}_D||, \tag{28}$$

where $\mathbf{r}_B$ and $\mathbf{r}_D$ are the position vectors of the centers of pin and bushing, respectively.

After the pin and bushing geometry is updated and the clearance size adjusted to reflect the wear, another dynamic analysis is performed. The wear depth is then computed based on the result of the new dynamic analysis. The geometry and the clearance size are once again updated. This process is iterated over the desired number of cycles. The process is summarized in the flowchart shown in Fig. 9.

5. Demonstration of the integration process and experiments for model validation

The integrated model is used here to predict the wear occurring at the crank-follower joint of a slider-crank mechanism (Fig. 10). Simulation results are compared to experimental data. This serves as both a demonstration of the integration model as well as a validation of the process.

The goal of the experimental test is to determine the wear that occurs at the joint between the crank and follower after several thousand revolutions of the crank. This joint consists of a pin that is attached to the crank and a bushing attached to the follower (the driven-link or follower). The pin is made of hardened steel and is

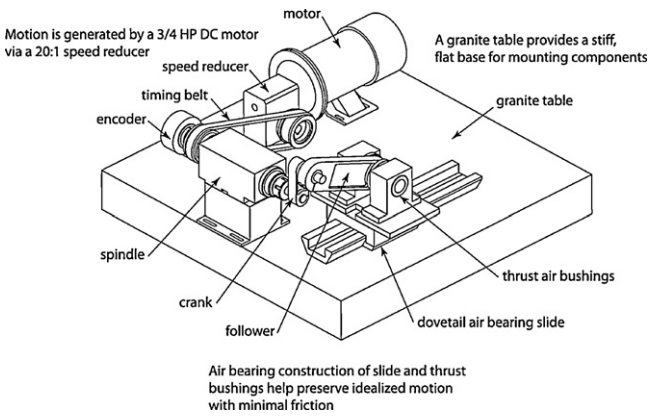

Fig. 10. Experimental apparatus for slider-crank mechanism.

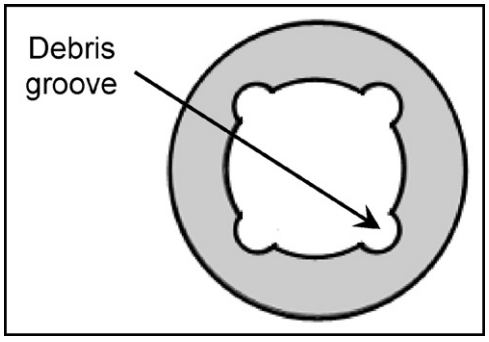

Fig. 11. Bushing with debris grooves.

assumed to be hard enough so that no appreciable wear occurs on its surface. The bushing, on the other hand, is made of polytetrafluoroethylene (PTFE) which is soft and is subject to considerable wear. To enable the wear debris to escape the contact area and prevent them from affecting the progression of wear, grooves were machined into the bushing. A diagram of the bushing is shown in Fig. 11.

In order to increase the joint reaction force and accelerate wear, the setup included the capability to attach a spring to the slider. The spring also ensured that the pin maintained contact with the bushing at all times. The slider-crank mechanism was designed and constructed to minimize friction and wear (to a negligible amount) at all joints except at the joint of interest (joint between crank and follower). This was achieved by using air bearing at the joints between the follower and slider and between the slider and ground [42]. The dimensions and mass parameters for the experimental slider-crank are shown in Table 3. Other test parameters including the friction and wear coefficient, crank velocity, and spring constant are provided in Tables 4 and 5.

To validate the integrated model, experimental results are compared to simulation results. In both cases, 21,400 crank cycles were executed. In Fig. 12, the joint reaction force at the non-ideal joint is compared. It is seen that the simulation closely predicts the reaction force except for some peaks that occurs at half crank rotation. These peaks are attributed to the direction change when the slider briefly

Table 3
Dimensions and mass properties of the slide-crank mechanism.

	Length (m)	Mass (kg)	Inertia ($\times 10^{-6}$ kg m^2)
Crank	0.0381	0.4045	204.0
Follower	0.1016	0.8175	5500.0
Slider	–	5.5487	–

Table 4
Properties of the pin and bushing.

	Pin	Bushing
Initial radius	9.525 mm	9.535 mm
Poisson's ratio	0.29	0.38
Young's modulus	206.8 GPa	0.139 GPa

Table 5
Test and simulation parameters.

Properties	Value
Crank (link-1) velocity	30 rpm
Spring constant	525.4 N/m
Friction coefficient	0.15
Wear coefficient [39]	5.05×10^{-4} mm^3/Nm

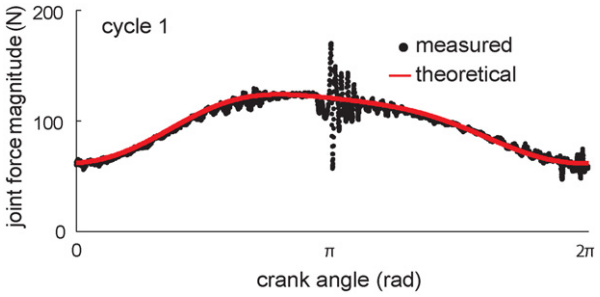

Fig. 12. Experimental and simulation results for initial joint reaction force.

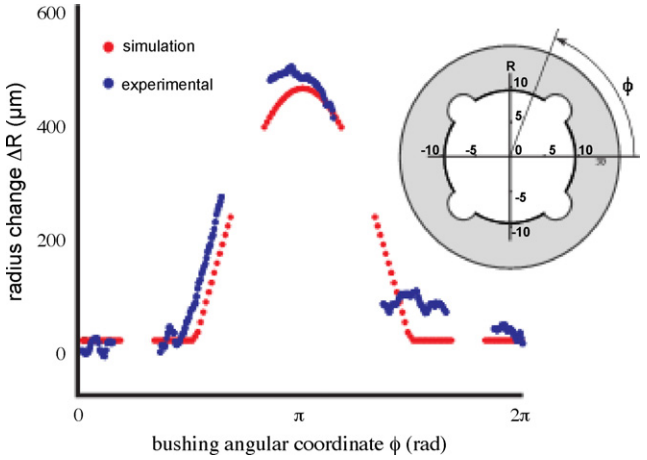

Fig. 13. Comparison of the wear on the bushing (the numbers on the ordinate are in micrometers).

impacts the sliding rail and resulting in the higher order dynamics. However, these peaks do not appreciably affect wear calculation because the sliding distance at this location is very small. Comparison of the wear on the bushing and the worn profile is shown in Fig. 13. In Table 6, the worn mass as well as the maximum wear depth for both the experiment and the simulation is compared. For both quantities the simulation provides a reasonably accurate prediction.

Table 6
Wear results from simulation and experiment (21,400 crank cycles).

	Experimental wear test	Simulation wear test	Error
Worn mass	0.1714 g	0.1589 g	7.2%
Max wear depth	0.4850 mm	0.4524 mm	6.7%

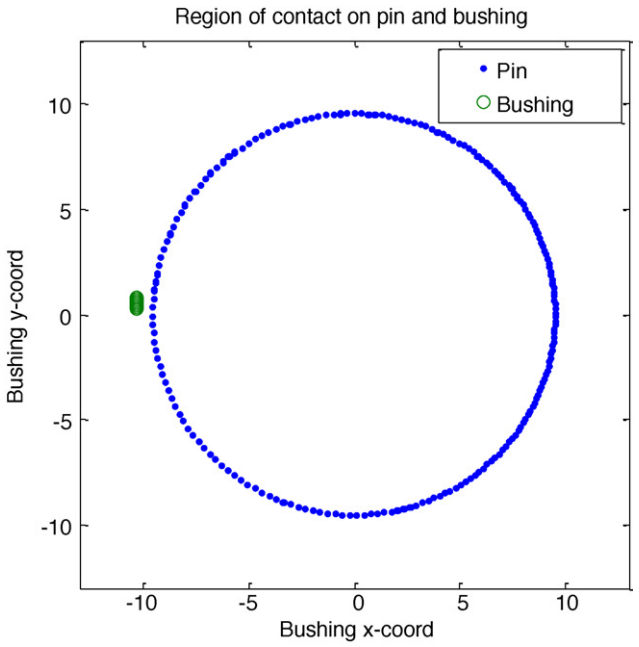

Fig. 14. Location of contact point *C* as predicted by the integrated model.

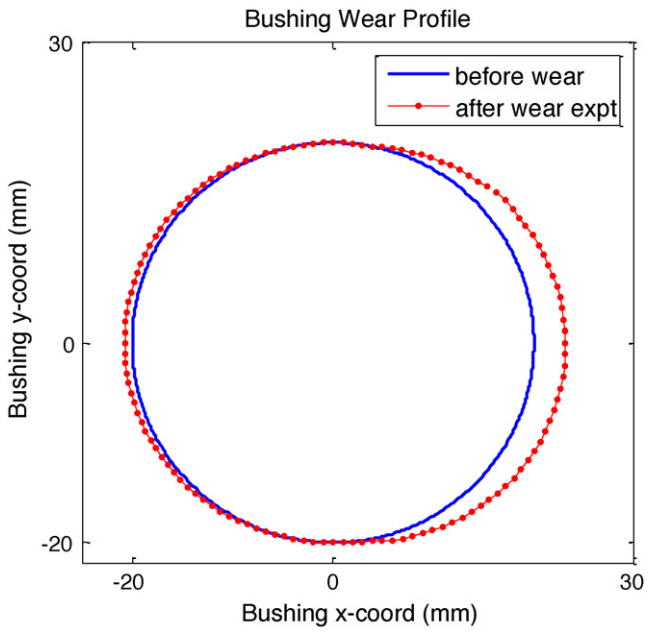

Fig. 16. Wear profile on the bushing for the slider-crank describe in Tables 1 and 2.

It was mentioned earlier that wear prediction at a non-ideal joint requires a multibody framework. This is because the location of contact and thus the region of wear cannot be otherwise determined. In the validation tests the correct contact locations were predicted. In Fig. 13, the maximum wear is seen to occur at about π angle (in the bushing angular coordinate) for both the experiment and the simulation. In terms of the dynamic analysis, this contact location corresponds to point *C* (as defined in Fig. 4). The plot of the contact point *C*, for a complete crank cycle, is shown in Fig. 14. This plot further confirms that the region of maximum wear would be on the left side of the bushing and thus correctly predicted.

It should be mentioned that the region of wear in the validation tests were restricted to one side of the bushing. This occurrence is indeed specific to this system particularly because a pre-tensioned spring was attached to the slider. For other systems the wear may not be restricted to one location. In such a case the need for wear prediction in a multibody dynamics framework becomes immediately apparent (since the location of contact would have to be determined through a dynamic analysis). An example of this is the slider-crank with parameters shown in Tables 1 and 2. This mechanism is larger (greater inertia) than the one used in the validation and no spring is attached to the slider. As a result wear on the bushing is expected to occur at various locations on the bushing. This is initially evident from the plot of contact point *C* for this system as seen in Fig. 15. The location of contact is concentrated on both halves of the bushing in contrast to the previous case. Results from a wear analysis for this case are shown in Fig. 16, which provides further confirmation.

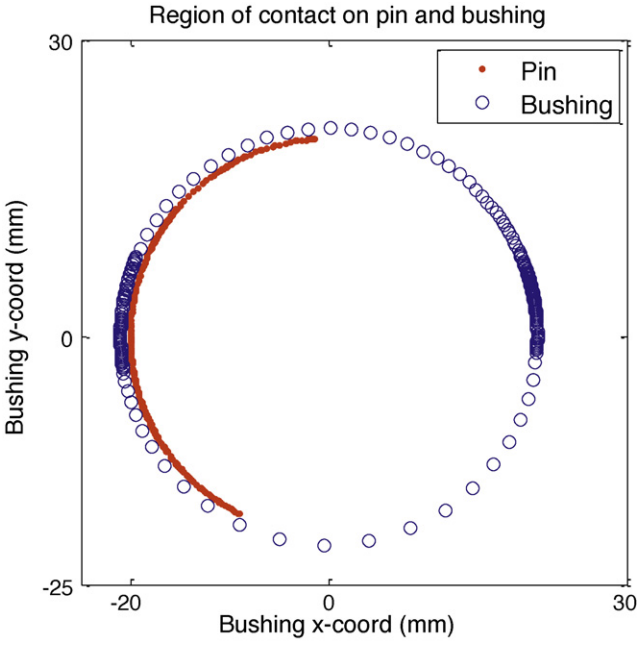

Fig. 15. Location of contact point *C* as predicted by the integrated model for slider-crank describe in Tables 1 and 2.

6. Summary and concluding remark

A procedure to analyze planar multibody systems experiencing wear at the revolute joint was presented. The procedure incorporates the effects of non-ideal revolute joint and therefore includes joint clearance. Unlike the ideal joint which uses kinematic constraints to restrict the motion of the joint components, the non-ideal joint uses force constraints to guide the motion of the joint components. The procedure assumes that the joint components can exhibit one of three configurations: (1) free-flight; (2) impact; and (3) following motion. In the case of the free-flight, no contact occurs between the components. This situation is modeled by requiring zero contact/reaction force so that no restriction is imposed on the motion of the joint components. For the impact and following motion, contact between the joint components is established. Contact force is developed based on the amount of penetration experienced during contact. By applying the contact force on the opposing joint components, the force constraints are enforced. Wear can then be incorporated by allowing the contact surfaces of the joint components to evolve while iteratively performing the dynamic analysis. The evolution is dictated by an iterative wear prediction procedure which estimates wear based on the joint reaction force and the relative sliding distance between the joint components.

The procedure was demonstrated using a slider-crank mechanism that experiences wear at a single joint. Wear predictions from the analysis show reasonable agreement with those from an experimental slider-crank mechanism. Another analysis was conducted to emphasize the need for performing wear prediction (for such systems) in a multibody dynamics framework. The main issue is that the location of contact (between the joint components) cannot be determined beforehand, but requires an analysis of the entire system.

Acknowledgements

The authors gratefully acknowledge support by the National Science Foundation (DMI-0600375) and Deere & Company.

References

[1] S. Dubowsky, On predicting the dynamic effects of clearances in planar mechanisms, ASME, Journal of Engineering for Industry (1974) 317–323.
[2] S. Dubowsky, F. Freudenstein, Dynamic analysis of mechanical systems with clearances. Part 1. Formulation of dynamic model, ASME, Journal of Engineering for Industry (1971) 305–309.
[3] S. Dubowsky, T.N. Gardner, Design and analysis of multilink flexible mechanisms with multiple clearance connection, ASME, Journal of Engineering for Industry (1977) 88–96.
[4] S.W.E. Earles, C.L.S. Wu, Motion analysis of a rigid link mechanism with clearance at a bearing using Lagrangian mechanics and digital computation, Mechanisms (1973) 83–89.
[5] C.L.S. Wu, S.W.E. Earles, A determination of contact-loss at a bearing of a linkage mechanism, Journal of Engineering for Industry, Series B 99 (2) (1977) 375–380.
[6] T. Furuhashi, N. Morita, M. Matsuura, Research on dynamics of four-bar linkage with clearances at turning pairs. 1st Report: general theory using continuous contact model, JSME 21 (1978) 518–523.
[7] N. Morita, T. Furuhashi, M. Matsuura, Research on dynamics of four-bar linkage with clearances at turning pairs. 2nd Report: analysis of crank-lever mechanism with clearance at joint of crank coupler using continuous contact model, JSME 21 (1978) 1284–1291.
[8] N. Morita, T. Furuhashi, M. Matsuura, Research on dynamics of four-bar linkage with clearances at turning pairs. 3rd Report: analysis of crank-lever mechanism with clearance at joint of coupler and lever using continuous contact model, JSME 21 (1978) 1292–1298.
[9] T. Furuhashi, N. Morita, M. Matsuura, Research on dynamics of four-bar linkage with clearances at turning pairs. 4th Report: forces acting at joints of crank-lever mechanism, JSME 21 (1978) 1299–1305.
[10] F. Farahanchi, S.W. Shaw, Chaotic and periodic dynamics of a slider-crank mechanism with slider clearance, Journal of Sound and Vibration 177 (3) (1994) 307–324.
[11] J. Rhee, A. Akay, Dynamic response of a revolute joint with clearance, Mechanisms Machine Theory 31 (1) (1996) 121–134.
[12] Y.A. Khulief, A.A. Shabana, Dynamic analysis of constrained system of rigid and flexible bodies with intermittent motion, Journal of Mechanisms, Transmissions, and Automations in Design 108 (1986) p.38–45.
[13] P. Ravn, A Continuous Analysis Method for Planar Multibody Systems with Joint Clearance, Multibody Systems Dynamics, vol. 2, Kluwer Academic Publishers, 1998, pp. 1–24.
[14] P. Flores, J. Ambrósio, P.J. Claro, Dynamic analysis for planar multibody mechanical systems with lubricated joints, Multibody System Dynamics 12 (2004) 47–74.
[15] P. Ravn, S. Shivaswamy, B.J. Alshaer, H.M. Lankarani, Joint clearances with lubricated long bearings in multibody mechanical systems, Journal of Mechanical Design 122 (2000) 484–488.
[16] P. Flores, J. Ambrósio, Revolute joints with clearance in multibody systems, Computers and Structures 82 (2004) 1359–1369.
[17] P. Flores, Dynamic analysis of mechanical systems with imperfect kinematic joints, Ph.D. Thesis, Minho University (Portugal), Guimarães, 2004.
[18] P. Flores, J. Ambrósio, J.C.P. Claro, H.M. Lankarani, C.S. Koshy, A study on dynamics of mechanical systems including joints with clearance and lubrication, Mechanism and Machine Theory 41 (2006) 247–261.
[19] P.E. Nikravesh, Computer-Aided Analysis of Mechanical System, Prentice-Hall, Englewood Cliffs, NJ, 1988.
[20] E.R. Haug, Computer-Aided Kinematics and Dynamics of Mechanical Systems, Needham Heights, MA, USA, Allyn and Bacon, 1989.
[21] M.L. Hamid, E.N. Parviz, Continuous Contact Force Model for Impact Analysis in Multibody Systems, Nonlinear Dynamics, vol. 5, Kluwer Academic Publishers, 1994, pp. 193–207.
[22] T.L. Schmitz, J.E. Action, J.C. Ziegert, W.G. Sawyer, The difficulty of measuring low friction: uncertainty analysis for friction coefficient measurement, Journal of Tribology 127 (2005) 673–678.
[23] W.G. Sawyer, Wear predictions for a simple-cam including the coupled evolution of wear and load, Lubrication Engineering (2001) 31–36.
[24] T.A. Blanchet, The interaction of wear and dynamics of a simple mechanism, Journal of Tribology 119 (1997) 597–599.
[25] N.H. Kim, D. Won, D. Burris, B. Holtkamp, G.R. Gessel, P. Swanson, W.G. Sawyer, Finite element analysis and experiments of metal/metal wear in oscillatory contacts, Wear 258 (2005) 1787–1793.
[26] M. Oqvist, Numerical simulations of mild wear using updated geometry with different step size approaches, Wear 249 (2001) 6–11.
[27] P. Podra, S. Andersson, Wear simulation with the Winkler surface model, Wear 207 (1997) 79–85.
[28] P. Podra, S. Andersson, Finite element analysis wear simulation of a conical spinning contact considering surface topography, Wear 224 (1999) 13–21.
[29] P. Podra, S. Andersson, Simulating sliding wear with finite element method, Tribology International 32 (1999) 71–81.
[30] A. Flodin, S. Andersson, Simulation of mild wear in spur gears, Wear 207 (1997) 16–23.
[31] A. Flodin, S. Andersson, A simplified model for wear prediction in helical gears, Wear 249 (2001) 285–292.
[32] J. Brauer, S. Andersson, Simulation of wear in gears with flank interference—a mixed FE and analytical approach, Wear 254 (2003) 1216–1232.
[33] A. Hugnell, S. Andersson, Simulating follower wear in a cam-follower contact, Wear 179 (1994) 101–107.
[34] A.B.-J. Hugnell, S. Björklund, S. Andersson, Simulation of the mild wear in a cam-follower contact with follower rotation, Wear 199 (1996) 202–210.
[35] N. Nayak, P.A. Lakshminarayanan, M.K.G. Babu, A.D. Dani, Predictions of cam follower wear in diesel engines, Wear 260 (2006) 181–192.
[36] B.J. Fregly, W.G. Sawyer, M.K. Harman, A.S. Banks, Computational wear prediction of a total knee replacement from in vivo kinematics, Journal of Biomechanics 38 (2005) 305–314.
[37] T.A. Maxian, T.D. Brown, D.R. Pedersen, J.J. Callaghan, A sliding-distance coupled finite element formulation for polyethylene wear in total hip arthroplasty, Journal of Biomechanics 29 (1996) 687–692.
[38] S.L. Bevill, G.R. Bevill, J.R. Penmetsa, A.J. Petrella, P.J. Rullkoetter, Finite element simulation of early creep and wear in total hip arthroplasty, Journal of Biomechanics 38 (2005) 2365–2374.
[39] T.L. Schmitz, J.E. Action, D.L. Burris, J.C. Ziegert, W.G. Sawyer, Wear-rate uncertainty analysis, ASME, Journal of Tribology 126 (4) (2004) 802–808.
[40] L.J. Yang, A test methodology for determination of wear coefficient, Wear 259 (2005) 1453–1461.
[41] S. Mukras, N.H. Kim, W.G. Sawyer, D.B. Jackson, L.W. Bergquist, Numerical integration schemes and parallel computation for wear prediction using finite element method, Wear 266 (7–8) (2009) 822–832.
[42] N. Mauntler, N.H. Kim, W.G. Sawyer, T.L. Schmitz, An instrumented crank-slider mechanism for validation of a combined finite element and wear model, in: Proceedings of 22nd Annual Meeting of American Society of Precision Engineering, October 14–19, Dallas, TX, 2007.
[43] ESDU-78035 Tribology Series, Contact Phenomena I: Stresses, Deflections and Contact Dimensions for Normally Loaded Unlubricated Elastic Components, Engineering Sciences Data Unit, London, 1978.